INFLUENCE OF RADIUS VARIATION ON THE DRY BUNDLE STRENGTH OF BRITTLE FIBRES

Ian J. Davies
Department of Mechanical Engineering, Curtin University of Technology,
GPO Box U1987, Perth, WA 6845, Australia

Keywords: *Brittle Fibres, Bundle Strength, Weibull Statistics, Fibre Radius Variation*

Abstract

The influence of radius variation on the dry bundle behaviour of brittle fibres was analysed using a Monte Carlo procedure. Unlike previous researchers, the present work obtained the strength of individual fibres directly from the flaw population assumed to be present on the fibre surface. The "tails" of the normalised load-displacement curves were noted to increase in magnitude as the radius variation increased whilst the fraction of fibres that failed at maximum load (0.201~0.204) was approximately 10% lower than expected from standard theory and noted to decrease slightly as the radius variation increased. Fibre radius distributions taken from the initial random selection of radii, and then at the point of maximum load, indicated the preferred failure of larger radius fibres; this effect was attributed to the larger number of flaws present on the surface of larger radius fibres.

1 Introduction

The requirement for lightweight structural materials in space and aerospace applications above 1200 ^{o}C has led to the development of advanced monolithic ceramics such as silicon carbide (SiC) and silicon nitride (Si_3N_4). Whilst they possess many advantages compared to lightweight superalloys, a serious disadvantage of monolithic ceramics is their relatively low fracture toughness, K_{IC}, when compared to that of most alloys (typically >100 MPa·m$^{1/2}$). For example, the fracture toughness of monolithic SiC is typically 1~3 MPa·m$^{1/2}$ whilst that of Si_3N_4 containing elongated β grains may reach 10~15 MPa·m$^{1/2}$.

One method to overcome this low fracture toughness (and associated brittle fracture behaviour and low reliability) has been through the introduction of ceramic matrix composites (CMCs), in which ceramic particles, whiskers, or fibres are incorporated into a ceramic matrix. For example, the incorporation of 30 mass% of chopped Tyranno® Si-Al-C (SA) fibres (mean length: 394 μm) increased the fracture toughness of monolithic SiC from 2.6

Table 1. Radius variation data for ceramic fibres based on the silicon carbide system.

Fibre type	Investigated fibre length, L (mm)	Mean radius, r_o (μm)	Minimum / maximum radius (μm)	Fractional radius variation, r_v	Reference
Tyranno® ZMI (Si-C-O)	500	5.5	2.78 / 7.22	0.40	Morimoto[3]
Tyranno® SA (SiC)	300	4.7	2.7 / 7.05	0.46	Youngblood *et al.*[4]
Nicalon™ (Si-C-O)	-	8.0	4 / 11	0.44	Zhu *et al.*[5]
Hi-Nicalon™ (Si-C-O)	250	6.9	3.9 / 10.1	0.45	Youngblood *et al.*[4]
Hi-Nicalon™ S (SiC)	300	6.15	4.3 / 7.3	0.24	Youngblood *et al.*[4]
Sylramic™ (SiC)	300	4.6	3.1 / 7.45	0.47	Youngblood *et al.*[4]
Tyranno® LoxM (Si-C-O)	-	4.03	2.13 / 5.72	0.45	Davies *et al.*[6]

MPa·m$^{1/2}$ to 5.8 MPa·m$^{1/2}$ [1]. Although a significant increase, fracture toughness values approaching those of metal alloys can only be approached through the use of relatively complicated and expensive CMCs based on multi-directional braided, woven, or knitted continuous fibres (*e.g.*, 40 MPa·m$^{1/2}$ for a 3D woven composite [2]).

One of the most important CMC systems has comprised of continuous SiC fibres within a SiC matrix produced from repeated polymer impregnation and pyrolysis (PIP) or chemical vapour infiltration (CVI). The SiC-based fibres for these composites have typically been 10 μm in diameter and either amorphous, nanocrystalline, or crystalline in structure.

Several researchers [3-6] have noted that modern SiC fibres, instead of having a constant radius along the fibre length, instead possess a "waviness" which can be approximated by a sinusoidal radius variation superimposed upon the mean radius value, $\overline{r}$. Table 1 illustrates radius variation data for several SiC fibres [3-6] and it is clear that the fractional radius variation, r_v, is significant and typically in the range of 0.25~0.50.

It would be expected that such a dramatic variation in fibre radius along the length may have significant consequences for the properties of the individual fibres, fibre bundles, and resulting composites. Several researchers have investigated this phenomenon (*e.g.*, [7]) whilst the present author has previously determined the mean strength, $\overline{\sigma}_S^*$, of a population of fibres with varying radii and whose strength is controlled by a population of surface flaws, to be of the form [8]:

$$\overline{\sigma}_S^* = \frac{\sigma_o(\overline{r})\Gamma\left[1+\frac{1}{m}\right]\overline{r}^{\frac{1}{m}}}{\Delta r\sqrt{2\pi}}\int_0^{\infty} r^{-\frac{1}{m}} e^{-\frac{1}{2}\left(\frac{r-\overline{r}}{\Delta r}\right)^2} dr \qquad (1)$$

where Δr is the Gaussian width of the radii distribution, m is the Weibull modulus, Γ is the gamma function, and $\sigma_o(\overline{r})$ is the characteristic scale strength at $\overline{r}$.

The present author has also investigated the initial creep rate [9, 10] and creep rupture time [10] of individual ceramic fibres with a varying radius along their length. For example, a ceramic fibre with a creep stress exponent of 3, which is typically the upper limit for current ceramic fibres based on the silicon carbide system [11], was found to have a normalised initial creep rate, $\dot{\varepsilon}^*$, *i.e.*, when compared to a fibre with a constant radius, $\overline{r}$, of [9]:

$$\dot{\varepsilon}^* = \frac{r_v^4 + 10r_v^2 + 5}{5\left(1-r_v^2\right)^5} \qquad (2)$$

for a fibre with a radius that varied linearly in the range $\overline{r} \pm r_v$ along the fibre length and [9]:

$$\dot{\varepsilon}^* = \frac{15r_v^4 + 40r_v^2 + 8}{8\left(1-r_v^2\right)^{11/2}} \qquad (3)$$

for a fibre with a sinusoidal variation in radius within the range $\overline{r} \pm r_v$ along the fibre length.

In the present work the author has utilized a Monte Carlo simulation method to extended the work of previous authors [12-16] in order to investigate the fracture behaviour of dry fibre bundles. The analysis assumed a population of fibres with a Gaussian distribution of fibre radii for neighbouring fibres but with each fibre having a constant fibre radius along its entire length. The presence of fibre radius distributions between neighbouring fibres in a single plane (perpendicular to the main axis of the fibre bundle) has been confirmed for Tyranno® LoxM Si-Ti-C-O fibres [17] and would closely approximate the situation in a CMC where a macroscopic crack has bridged a fibre bundle, *i.e.*, constant radius within each fibre but different radii between neighbouring fibres.

An important extension when compared to the analysis of previous researchers is that the strength of each fibre was calculated after taking into account the flaw population present within the fibre, rather than by directly assuming a distribution of macroscopic strength (normally taken to be a Weibull distribution [18]). The correlation between microscopic flaw population and macroscopic mechanical behaviour for a collection of brittle fibres was achieved using the analysis of Jayatilaka and Trustrum [19].

2 Experimental Procedure

In this work a Monte Carlo simulation was employed in order to investigate the influence of radius variation on the dry bundle strength of brittle fibres. All the simulations were carried out, unless otherwise stated, on a collection of 10^4 fibres for

each bundle. Following the procedure of Jayatilaka and Trustrum [19], the fibres were considered to contain a population of flaws with a probability density, *f(a)*, given by [20]:

$$f(a) = \frac{c^{n-1}}{(n-1)!} a^{-n} e^{-c/a} \quad (4)$$

where a is half the flaw length, c is a scaling parameter (of similar scale to the mean flaw size), and n is the rate at which $f(a)$ tends to zero for large a. The distribution of $f(a)$ for the case of $c = 10^{-6}$ m and $n = 3$ utilised in the present work has been shown in Fig. 1. Assuming the flaws to be inclined with a random angle, β, the strength for any given flaw can be determined using the following relationship [19]:

$$\sigma = \frac{K_{IC}}{\sqrt{2a\beta}} \quad (5)$$

where K_{IC} is the fracture toughness. A value of 1 MPa·m$^{1/2}$ was chosen as a typical value for ceramic fibres [21]. However, it should be noted that the particular values of K_{IC}, c, and n chosen would have no influence on the general trends noted in this investigation.

Jayatilaka and Trustrum [19] showed that, when taking into account the limits of integration, the probability of failure at any given stress, $F(\sigma)$, can be given by:

$$F(\sigma) = \int_{\frac{K_{IC}^2}{\pi\sigma^2}}^{\infty} \left[1 - \frac{K_{IC}^2}{\pi a \sigma^2}\right] \frac{c^{n-1} a^{-n} e^{-c/a}}{(n-2)!} da \quad (6)$$

which was found to be approximated by:

$$F(\sigma) = \frac{\Psi^{n-1}}{n!}\left[1 - \Psi\left(\frac{n-1}{n+1}\right) + O\Psi^2\right] \quad (7)$$

where:

$$\Psi = \left(\frac{\pi\sigma^2 c}{K_{IC}^2}\right) \quad (8)$$

From comparison with the simplified Weibull equation [18]:

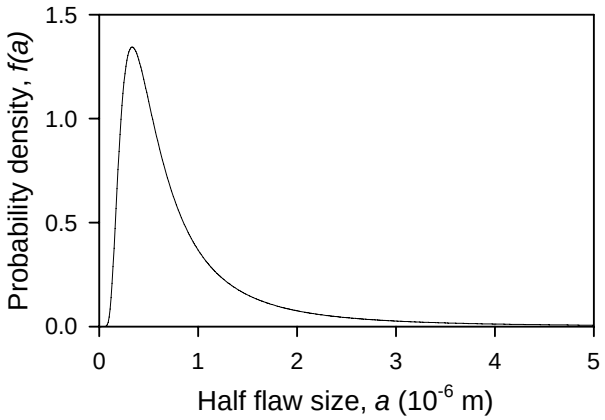

Fig. 1. Schematic illustration of the Poloniecki and Wilshaw [20] flaw size distribution for the case of $c = 10^{-6}$ m and $n = 3$.

$$F(\sigma) = 1 - e^{-\left(\sigma/\sigma_o\right)^m} \quad (9)$$

it was deduced that the value of n in $f(a)$ could be related to the Weibull modulus, m, through [19]:

$$m = 2n - 2 \quad (10)$$

Thus, the value of $n = 3$ chosen in this work was thus equivalent to a Weibull modulus of 4, which is typical for ceramic fibres based on the silicon carbide system [22].

In the present work it was decided to make the number of flaws proportional to the surface area for the brittle fibres under investigation; this being a reasonable assumption for most brittle materials. The number of flaws within a fibre with a radius equal to the mean value, $\bar{r}$, was taken to be 10^4 in order to ensure a reasonable statistical representation of the flaw population for any given fibre. As mentioned previously, the variation in radii between neighbouring fibres was assumed to follow a Gaussian distribution, $G(r)$, as follows:

$$G(r) = \frac{1}{\Delta r\sqrt{2\pi}} e^{-\frac{1}{2}\left(\frac{r-\bar{r}}{\Delta r}\right)^2} \quad (11)$$

For each of the 10^4 fibres within the dry bundle, a random fibre radius was chosen according to $G(r)$ and the number of flaws calculated according to:

$$\text{Number of flaws} = 10^4\left(\frac{r}{\bar{r}}\right) \quad (12)$$

For each of the flaws within the fibre surface, a random half flaw size was chosen according to *f(a)* and a random value of β chosen in the range (due to symmetry) of $0 \le \beta \le \pi/2$ with the associated flaw strength being calculated according to Eq. 5. The strength of each fibre was thus taken to be that of the weakest flaw present within each of the fibres. In order to achieve a statistically representative result, great care was taken in generating the (pseudo) random numbers utilised in this work with a linear congruent method being chosen for this procedure.

In order to examine the effectiveness of the current Monte Carlo simulation, a Weibull curve generated by the current simulation for individual fibres with no radius variation (in order to exclude any effect due to this parameter) has been presented in Fig. 2 together with a curve generated using the theory of Jayatilaka and Trustrum [19]. A comparison of the Weibull parameters for these curves has been shown in Table 2. It can be seen from Fig. 2 and Table 2 that the Monte Carlo simulation was able to effectively describe the statistical mechanical behaviour of a population of brittle fibres using the Jayatilaka and Trustrum model [19] as the theoretical framework.

Following confirmation of the efficacy of the current analysis, the next step was to investigate the load-displacement behaviour of the dry fibre bundles as a function of Gaussian radius width; both the maximum load and displacement at maximum load were normalised with respect to the case of a fibre bundle containing constant radius fibres. In the present work a global load sharing rule was applied to the distribution of load with the fibre bundle following fracture of any fibre.

If we consider the respective surface area, *SA(r)*, and area, *A(r)*, of two example fibres with radii $\bar{r} - \delta r$ and $\bar{r} + \delta r$ then:

$$\frac{SA(\bar{r} - \delta r) + SA(\bar{r} + \delta r)}{2} = SA(\bar{r}) \qquad (13)$$

Table 2. Comparison of parameters obtained from the simulated and theoretical Weibull curves.

Parameter	Simulation	Theory
m	4.074	4.000
σ_o	88.15	88.30
Spearman correlation coefficient	>0.99997	

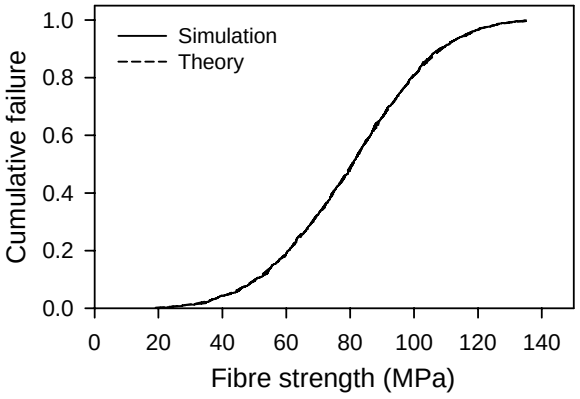

Fig. 2. Comparison between simulated data and theoretical expression derived by Jayatilaka and Trustrum [19] for the following conditions: Number of fibres = 10^3, Flaws per fibre = 10^4, K_{IC} = 10^6 MPa·m$^{1/2}$, n = 3, and c = 10^{-6} m.

and

$$\frac{A(\bar{r} - \delta r) + A(\bar{r} + \delta r)}{2} > A(\bar{r}) \qquad (14)$$

which means that, for a dry bundle containing a constant number of fibres, N_f, with a distribution of radii, the surface area of the fibre bundle will remain constant whilst the area (*i.e.*, volume fraction, V_f) will increase. Therefore, properties obtained from the load-displacement curves, such as maximum load, were determined in terms of both constant N_f and constant V_f.

3 Results and Discussion

3.1 Load-Displacement Curves

The influence of Gaussian radius width on typical load-displacement curves for dry bundles containing 10^4 brittle fibres has been presented in Fig. 3. Whereas there was no apparent influence of radius variation on the shape of the load-displacement curve prior to the point of maximum load, a small but measurable effect was noticed in the "tail" of the load-displacement curves as the normalised load started to decrease. For this situation, the presence of a radius variation produced a relatively higher sustained load. Whilst this effect was judged to be significant and able to double the relative normalised load for the case of a fibre bundle with Δr = 0.3 when compared to a constant radius fibre bundle, however, when compared to the

maximum load achieved, the magnitude of the load increase in the tail region due to radius variation was still relatively minor and on the order of 3~4% of the maximum load.

3.2 Fibre Radius Distributions

In order to investigate the influence of radius variation on the dry bundle behaviour of brittle fibres, distributions of fibre radii normalised to $\overline{r}$ have been presented in Fig. 4. As expected, the initial distribution of radii data (prior to the simulated loading) was essentially Gaussian in nature with a small amount of superimposed noise consistent with the number of fibre radii sampled, *i.e.*, 10^6. In contrast to this, the radius distribution for fibres at the point of maximum load was no longer symmetrical about the normalization point, *i.e.*, $r = \overline{r}$, but instead exhibited a slightly higher drop for higher radius values ($\overline{r}+\delta r$) when compared to lower radii fibres ($\overline{r}-\delta r$). Also shown in Fig. 4 is the ratio of these two distributions as a function of r with the ratio being seen to follow an essentially linear decreasing relationship as r increased. The data presented suggested that fibres with larger radii preferentially failed during loading of the fibre bundle.

At first consideration it may appear that the higher numbers of flaws per unit cross-sectional area for fibres with smaller radii (due to the larger ratio of surface area to fibre volume as r decreases) should lead to fibres with smaller radii being weaker. However, for global load sharing the load would be shared between each fibre in proportion to the fibre cross-sectional area, *i.e.*, constant stress.

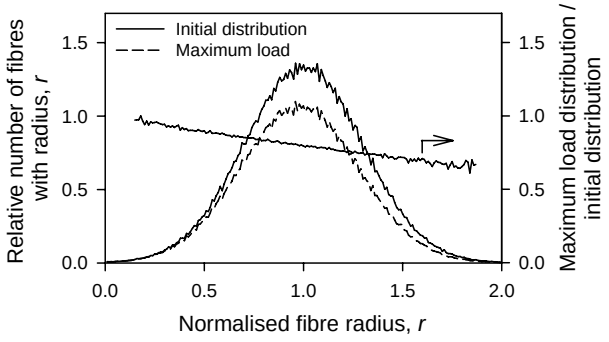

Fig. 4. Comparison between: (i) initial distribution of radii data for 10^6 fibres picked during simulation and (ii) radius distribution at the point of maximum load, with Δr = 0.3 for both cases. Also shown is the ratio between maximum load distribution and initial distribution.

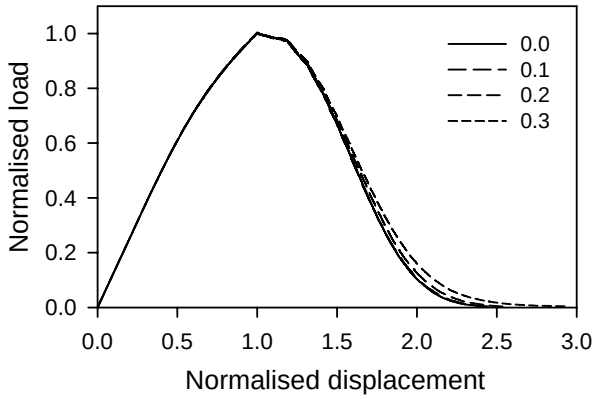

Fig. 3. Influence of fibre radius Gaussian width, Δr, on normalised load-displacement curves for simulations conducted utilising 10^4 fibres, each containing 10^4 randomly oriented flaws.

Therefore, fibres with larger radii will have larger surface areas and therefore a larger number of flaws, making them more likely to have a larger maximum flaw size (strictly speaking, "effective" flaw size when also taking into account the angle, β) and thus have a lower strength, when compared to a fibre with a smaller radius.

This result may have some implications for composite researchers as, for a constant fibre/matrix interface shear strength, τ, the load sustained by the fibre bundle within the composite will be essentially proportional to the total fibre surface area. Thus, the increased probability of failure for fibres with larger radii will leave a remaining population with a smaller mean fibre radius; which equates to an increasing surface area per fibre and thus potentially a higher load per unit area (*i.e.*, volume fraction) of fibre. In a similar line of thought, the smaller number of flaws present along the length of a fibre with a reduced fibre radius may have a positive influence on the fibre pullout length which, all other things being kept constant, will tend to increase the fracture toughness of the composite.

3.3 Fraction of Failed Fibres

The influence of radius variation on the fraction of failed fibres, α, at the maximum load has been presented in Fig. 5 with a clearly defined, but small, trend being noted, *i.e.*, the fraction of fibres that failed up to the point of maximum load decreased, albeit slightly, with increasing radius variation. The range of values for the fraction of failed fibres noted in this work (0.201~0.204) was approximately 10% below the value (0.221)

calculated using the following expression [13]:

$$\alpha = 1 - e^{-\left(1/m\right)} \tag{15}$$

The reason behind this unexpectedly low value of α will be investigated in later work. However, whilst a definite trend in α was noted with a change in radius variation, this change was only up to a maximum of approximately 1.5% for the largest radius variation investigated.

3.4 Total Area, Flaws, and Maximum Load

The influence of radius variation on total cross-sectional area, total flaw numbers, and maximum load normalised to either a constant fibre number or constant cross-sectional area (*i.e.*, volume fraction) has been presented in Fig. 6. As expected from Eq. 14, for a constant fibre number, the normalised total cross-sectional area, A_T, increased with increasing radius variation with the expected relationship between A_T and Δr being of the form:

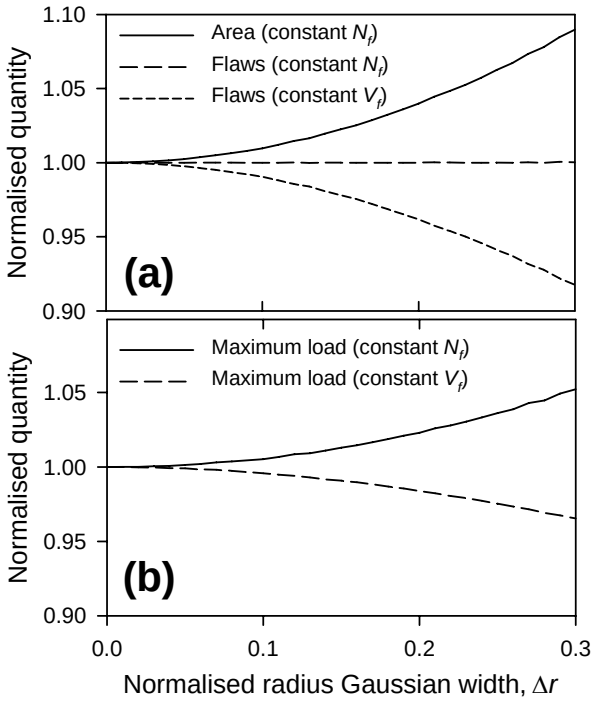

Fig. 6. Influence of normalised fibre radius Gaussian width, Δr, on simulation results for constant fibre number, N_f, and constant volume fraction, V_f, situations: (a) surface area and number of flaws, and (b) maximum load. Data was averaged from 500 simulations for each Δr.

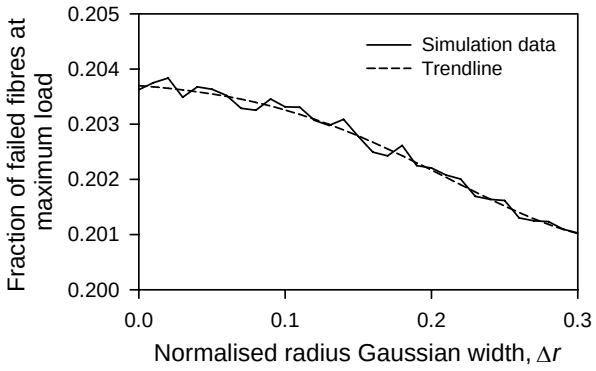

Fig. 5. Influence of normalised fibre radius Gaussian width, Δr, on the fraction of failed fibres at the maximum load. Data was averaged from 500 simulations for each Δr.

$$A_T = \frac{\bar{r}^2}{\Delta r\sqrt{2\pi}} \int_0^\infty r^2 e^{-\frac{1}{2}\left(\frac{r-\bar{r}}{\Delta r}\right)^2} dr \tag{16}$$

The normalised total flaw number, *FN*, within the fibre bundle was found to remain unchanged with respect to radius variation for the case of constant fibre numbers. This was explained through the relationship between radius and flaw number being linear for individual fibres as inferred by Eq. 13 and:

$$FN = \frac{\bar{r}}{\Delta r\sqrt{2\pi}} \int_0^\infty r e^{-\frac{1}{2}\left(\frac{r-\bar{r}}{\Delta r}\right)^2} dr = 1 \tag{17}$$

With regards to the trend in *FN* with radius variation for constant volume fraction, in this case the value of *FN* in Eq. 17 would be divided by A_T in Eq. 16 (to take into account the increasing A_T with increasing radius variation), resulting in the decrease of *FN* with radius variation for constant volume fraction.

Analysing the trend in maximum load for constant fibre number (Fig. 6(b)) showed an increase of approximately 5% as the radius variation increased. Most of the increase in maximum load was attributed to the increasing total cross-sectional area, *i.e.*, volume fraction, as the radius variation increased. Likewise, the decrease of approximately 4% in maximum load with increasing radius variation for a constant volume fraction was attributed to the maximum load being divided by A_T in Eq. 16 due to the need to take into account the constant volume fraction.

4 Conclusions

The mechanical behavior of dry fibre bundles were analysed using a Monte Carlo technique in order to investigate any possible influence of radius variation. Unlike most previous researchers, the present work obtained the strength of the individual fibres as a direct consequence of the flaw population assumed to be present on the fibre surface. The flaw number was normalised to a value of 10^4 for the case of a constant radius fibre, with each fibre bundle being considered to contain 10^4 fibres. The following conclusions were made:

(i) the "tails" of the normalised load-displacement curves were noted to increase in magnitude as the radius variation increased; however, when compared to the maximum load achieved this effect was relatively small (3~4%).

(ii) fibre radius distributions taken from the initial radius selection and then at the point of maximum load indicated the preferred failure of larger radius fibres; this effect was attributed to the increased number of flaws present on the surface of larger radius fibres.

(iii) the fraction of fibres (0.201~0.204) that failed at maximum load was approximately 10% lower than expected from standard theory and was noted to decrease slightly as the radius variation increased; this aspect will be the subject of additional research.

(iv) the normalised values of total cross-sectional area, total flaw number, and maximum load, for the case of a constant fibre number or volume fraction, were found to change as expected as the radius variation increased.

References

[1] Itatani, K., Tanaka, T., Suemasu, H., Nozue, A. and Davies, I. J., "Fabrication and fracture behaviour of silicon carbide composites containing chopped Tyranno® Si-Al-C fibre", *J. Australasian Ceram. Soc.*, Vol. 41, No. 1, pp. 1-7, 2005.

[2] Ishikawa, T., Yamamura, Y., Hirokawa, T., Hayashi, Y., Noguchi, Y. and Matsushima, M., "Strength and fracture toughness properties of oxidation resistant high-temperature ceramic matrix composites", *Proc. Ninth Int. Conf. Compos. Maters.*, London, U. K., pp. 137-144, 1993.

[3] Morimoto, T., "A representative diameter for the evaluation of brittle monofilament strength", *Proc. 9th US-Japan Conf. Compos. Maters.*, Mishima, Japan, pp. 265-272, 2000.

[4] Youngblood, G. E., Eiholzer, C. R., Lewinsohn, C. A., Jones, R. H., Hasegawa, A. and Kohyama, A., "Fiber diameter variation/sample preparation and analysis techniques", *Ceram. Eng. Sci. Proc.*, Vol. 20, No. 3, pp. 481-486, 1999.

[5] Zhu, Y. T., Taylor, S. T., Stout, M. G., Butt, D. P., Blumenthal, W. R. and Lowe, T. C., "On the statistical strength of Nicalon fibers and its characterization", *Ceram. Eng. Sci. Proc.*, Vol. 18, No. 3, pp. 119-126, 1997.

[6] Davies, I. J., Ishikawa, T., Shibuya, M., Hirokawa, T. and Gotoh, J., "Fibre and interfacial properties measured *in situ* for a 3-D woven SiC/SiC-based composite with glass sealant", *Composites: Part A*, Vol. 30, No. 4, pp. 587-591, 1999.

[7] Morimoto, T., "A representative diameter for the Weibull scaling of variable diameter monofilament strength", *Composites: Part A*, Vol. 34, pp. 597-601, 2003.

[8] Davies, I. J., "Effect of radius variation on the mean strength of brittle fibres", *J. Maters. Sci. Letts.*, Vol. 20, No. 12, pp. 1103-1105, 2001.

[9] Davies, I. J., "Effect of variable radius on the initial creep rate of ceramic fibres", *J. Maters. Sci.*, Vol. 40, No. 23, pp. 6187-6193, 2005.

[10] Davies, I. J. and Entwistle, R. D., "Influence of geometrical irregularities on the creep behaviour of ceramic fibres", *Ceram. Trans.*, Vol. 192, pp. 163-174, 2006.

[11] Bodet, R., Bourrat, X., Lamon, J. and Naslain, R., "Tensile creep behaviour of a silicon carbide-based fibre with a low oxygen content", *J. Maters. Sci.*, Vol. 30, No. 3, pp. 661-677, 1995.

[12] Daniels, H. E., "The statistical theory of the strength of bundles of threads", *Proc. Royal Soc. London*, Vol. A183, No. 995, pp. 405-435, 1945.

[13] Coleman, B. D., "On the strength of classical fibres and fibre bundles", *J. Mech. Phys. Solids*, Vol. 7, pp. 60-70, 1958.

[14] Phoenix, S. L., "Stochastic strength and fatigue of fiber bundles", *Int. J. Fracture*, Vol. 14, No. 3, pp. 327-344, 1978.

[15] Morimoto, T., "Statistics on the strength of ceramic fiber bundle", *Int. J. Maters. Prod. Technol.*, Vol. 16, No. 1-3, pp. 22-31, 2001

[16] Morimoto, T., "A statistical upper limit strength for ceramic fiber bundles", *Ceram. Eng. Sci. Proc.*, Vol. 22, No. 3, pp. 355-362, 2001.

[17] Davies, I. J. and Ishikawa, T., "Bundle to bundle variation of mean fibre radius for Tyranno® LoxM Si-Ti-C-O fibres", *J. Maters. Sci. Letts.*, Vol. 20, No. 6, pp. 505-507, 2001.

[18] Weibull W., "A statistical distribution function of wide applicability", *J. Appl. Mech.*, Vol. 18, pp. 293-297, 1951.

[19] Jayatilaka, A. De S. and Trustrum, K., "Statistical approach to brittle fracture", *J. Maters. Sci.*, Vol. 12, pp. 1426-1430, 1977.

[20] Poloniecki, D. and Wilshaw, T. R., "Determination of surface crack size densities in glass", *Nature*, Vol.

229, pp. 226-227, 1971.

[21] Davies, I. J. and Ishikawa, T., "Estimation of the fracture toughness of Tyranno® Si-Ti-C-O fibres from flaw size and 'fracture mirror' data measured in situ a 3-D woven SiC/SiC composite", *Int. J. Maters. Prod. Tech.*, Vol. 16, No. 1-3, pp. 189-196, 2001.

[22] Davies, I. J., Ishikawa, T., Shibuya, M. and Hirokawa, T., "Fibre strength parameters measured *in situ* for ceramic matrix composites tested at elevated temperature in vacuum and air", *Composites Sci. Technol.*, Vol. 59, No. 6, pp. 801-811, 1999.